Investigation of the production of neutron-rich isotopes in the multinucleon transfer reaction ^{197}Au + ^{238}U*

Dong-Hong Zhang (张冬红)[1,2,4†] Da-Long Jiang (姜大龙)[3]

[1]College of Physics and Electronic Science, Shanxi Datong University, Datong 037009, China
[2]The Key Laboratory of Beam Technology of the Ministry of Education, School of Physics and Astronomy, Beijing Normal University, Beijing 100875, China
[3]Nanchang Polytechnic University, Nanchang 330500, China
[4]Institute of Radiation Technology, Beijing Academy of Science and Technology, Beijing 100875, China

Abstract: The production mechanisms and cross sections for neutron-rich actinide nuclides formed in multinucleon transfer reactions with ^{238}U targets are systematically investigated using the dinuclear system (DNS) model coupled with the GEMINI++ de-excitation code. The tip-to-tip configurations for the ^{48}Ca+^{248}Cm and ^{238}U+^{238}U reactions are in good agreement with experimental data. Calculations of the potential energy surfaces and driving potentials for the three systems ^{197}Au+^{238}U, ^{186}W+^{238}U, and ^{232}Th+^{238}U indicate that the first two systems exhibit pronounced "inverse" quasifission characteristics due to shell effects. The final isotopic production cross sections of target-like fragments with Z=93-101 for the three systems are calculated at $E_{c.m.}$=1.10V_B. The results show that the production cross sections for the ^{197}Au+^{238}U system are significantly higher than those for the other two systems, with a particularly pronounced advantage in the Z=93-98 region. Further analysis of the ^{197}Au+^{238}U reaction at different incident energies reveals that higher incident energies are favorable in the Z=93-98 region, whereas lower energies are more advantageous in the Z=99-101 region. Calculations of the interaction time show that higher incident energies lead to longer contact times between the nuclei. Production cross sections are predicted for 61 previously unobserved neutron-rich nuclides with values greater than 1 pb, providing a theoretical basis for experimental synthesis.

Keywords: neutron-rich isotopes, multinucleon transfer, dinuclear system

DOI: 10.1088/1674-1137/ae6a84 **CSTR:**

I. INTRODUCTION

Synthesizing new nuclides and expanding the nuclear landscape is one of the core tasks in nuclear physics research. It is of great significance for exploring the limits of nuclear existence, understanding the rapid neutron capture process in astrophysics, testing and developing nuclear theory models. Since the 1970s, with the continuous improvement of detection techniques and accelerator performance, multinucleon transfer reactions have gradually become a frontier topic in nuclear physics research[1−4]. Compared with fusion-evaporation reactions, multinucleon transfer reactions can produce unknown nuclides far from the β-stability line through deep nucleon exchange between projectile and target in the near-barrier energy region, providing a unique experimental means for expanding the nuclide chart, exploring the “island of stability", and investigating the evolution of nuclear structure under extreme neutron numbers [5−7].

Experimentally, studies on multinucleon transfer reactions have evolved from light to heavy targets, and from symmetric to asymmetric systems. Early experiments mainly focused on light or medium-mass targets. For example, in the 1970s, the Joint Institute for Nuclear Research (JINR) research group systematically studied the synthesis of neutron-rich nuclides from carbon to thorium using projectiles such as ^{22}Ne and ^{40}Ar bombarding targets like ^{232}Th and ^{238}U[8−11]. Research groups at Orsay in France and Berkeley in the United States observed a large number of new nuclides in reactions such as ^{40}Ar+^{238}U and ^{84}Kr+^{209}Bi[12−16]. Entering the 21st century, with advancements in detection technology, multinucleon transfer experiments using projectiles such as ^{136}Xe,^{48}Ca,and ^{238}U have been successively carried out at laboratories including GSI, ANL, and JINR[17−19]. Among them, the ^{136}Xe+^{208}Pb system, in which both pro-

Received 8 April 2026; Accepted 6 May 2026

* This work is supported in part by the National Key R&D Program of China under Grant No. 2023YFA1606401 and the National Natural Science Foundation of China under Grants No. 12447135, No. 12135004, No. 11635003, No. 11961141004

† E-mail: zhdhsuccess@163.com

jectile and target possess magic or near-magic structures, has become a classic system for studying the synthesis of neutron-rich N=126 isotones[20−25].*Watanabe* et al. demonstrated that the production cross sections of N=126 isotones in the ^{136}Xe+^{198}Pt reaction are much larger than those measured in the fragmentation reaction of a ^{208}Pb beam[26]. Furthermore, studies on symmetric or near-symmetric heavy systems such as ^{238}U+^{238}U and ^{238}U+^{248}Cm have revealed mass drift and shell effects in deep-inelastic collisions between heavy nuclei[27−29].

Multinucleon transfer reactions with uranium as the target have gradually become an important route for synthesizing neutron-rich actinide nuclides due to their unique physical advantages. Uranium, as the heaviest stable nucleus in nature, possesses a high neutron-to-proton ratio (N/Z) and significant quadrupole deformation. As early as 2011, Texas A&M University conducted exploratory experiments on the ^{197}Au+^{232}Th reaction using the BigSol spectrometer, first observing indications of heavy nuclei with atomic numbers exceeding 97, laying the foundation for subsequent research[30]. Since then, several internationally renowned laboratories have carried out systematic experimental studies with uranium targets. The GSI Helmholtz Center for Heavy Ion Research in Germany performed experiments on the ^{48}Ca+^{238}U reaction at the SHIP velocity filter, successfully observing about 90 nuclides ranging from Tl to Am (Z=81-95), and identified the products with high precision through α, γ, and spontaneous decay activities[31]. ANL in the United States systematically investigated the ^{136}Xe+^{238}U reaction using the AGFA gas-filled separator combined with the Gammasphere high-purity germanium array, observing deep transfer processes with up to about 27 nucleons transferred from the projectile to the target, with the heaviest observed product having a mass number of about 265 u and cross sections on the order of a few hundred microbarns[32]. JINR in Russia successfully synthesized ^{273}Ds using the ^{40}Ca+^{238}U reaction, with an evaporation residue cross section of 0.18 pb[33]. These experiments consistently demonstrate that in the near-barrier energy region, collisions between a uranium target and deformed projectiles readily induce deep nucleon transfer, producing target-like fragments with atomic numbers Z lareger than 90. However, due to the complexity of the reaction mechanism and the generally low cross sections (on the order of microbarns to nanobarns), as well as limitations in experimental detection efficiency, there is a high demand for theoretical predictions of unknown nuclide yields and analysis of reaction mechanisms.

Various theoretical models have been developed to describe the dynamics of multinucleon transfer reactions. Examples include the improved quantum molecular dynamics (ImQMD) model[34−40], the time-dependent Hartree-Fock (TDHF) method[41−44], the dinuclear system (DNS) model[45−65], time-dependent covariant density functional theory (TD-CDFT)[66, 67], Langevin equations[68−71], the deep inelastic transfer (DIT) model[72], the coupled Langevin and master equation (CLIM) method[73], and the quantum diffusion approach based on the stochastic mean-field (SMF) theory[74−78]. These theories have their respective advantages in dealing with some specific issues in multinucleon transfer reactions. Among them, the DNS model describes the diffusion process of nucleon transfer by solving master equations, and can self-consistently treat mass and charge relaxation, energy dissipation, and shell effects between projectile and target. When coupled with the GEMINI++ de-excitation code to handle the decay of excited fragments[79, 80], the DNS model has achieved good agreement with experimental results in describing the product distribution of heavy-ion multinucleon transfer reactions. In particular, analyzing potential-energy surfaces and driving potentials can reveal the guiding role of shell effects on the nucleon transfer path, providing a theoretical basis for selecting optimal projectile-target combinations and incident energies.

Based on the DNS model combined with the GEMINI++ model, the production mechanism of heavy neutron nuclides near Z=93-101 will be investigated by calculating three projectile-target combinations: ^{197}Au+^{238}U, ^{186}W+^{238}U, and ^{232}Th+^{238}U for multinucleon transfer reactions. The orientation effects, optimal reaction system and incident energy for transuranium nuclides will be determined.

The structure of this article is organized as follows. Section **2** provides a brief introduction of the DNS model. The results and discussion are presented in Section **3**. Finally, the main conclusions are summarized in Section **4**.

II. THEORETICAL FRAMEWORK

The dinuclear system (DNS) model has been widely applied to describe the production of new nuclides in quasi-fission processes, fusion reactions, and multinucleon transfer reactions. After the projectile crosses the Coulomb barrier, it forms a dinuclear system with the target in the potential pocket. Nucleon transfer occurs at the bottom of the potential pocket, driving the evolution of the dinuclear system along the mass-asymmetry coordinate $\eta = \frac{(A_T - A_P)}{(A_T + A_P)}$. The potential energy surface (PES)[81] plays a pivotal role in nucleon-transfer processes and is defined as

$$U(Z_1, N_1, \theta_1, \theta_2, R_{\rm cont}) = \Delta(Z_1, N_1) + \Delta(Z_2, N_2) + V_{\rm CN}(Z_1, N_1, \theta_1, \theta_2, R_{\rm cont}). \quad (1)$$

Here, $\Delta(Z_i, N_i)$ $(i = 1, 2)$ denotes the mass excess of fragment i, where Z_i and N_i represent the proton and neutron

numbers of the ith fragment, respectively. The sum of Z_1 and Z_2 equals the total number of protons in the composite system, and likewise for neutrons. $V_{CN}(Z_1,N_1,\theta_1,\theta_2,R_{\rm cont})$ is the effective nucleus-nucleus interaction potential between the fragments, where θ_i is the angle between the symmetry axis and the collision axis of the ith fragment. $R_{\rm cont}$ denotes the position of the potential pocket in the nucleus-nucleus potential when potential pockets are included. In cases without an interaction potential, $R_{\rm cont}$ is given by: $R_{\rm cont}=R_1\left[1+\beta_2^{(1)}Y_{20}(\theta_1)\right]+R_2\left[1+\beta_2^{(2)}Y_{20}(\theta_2)\right]+0.7\,{\rm fm}$. $\beta_2^{(i)}$ $(i=1,2)$ denotes the quadrupole deformation parameter of fragment i and is taken from [82]. The mass excess can be expressed as

$$\begin{aligned}\Delta(Z,N)=&Z\Delta_p+N\Delta_n-a_v(1-\kappa I^2)A\\&+a_s(1-\kappa I^2)A^{2/3}+a_cZ^2/A^{1/3}\\&-c_4Z^2/A+E_{\rm pair}(Z_i,N_i)+E_{\rm shell}(Z_i,N_i).\end{aligned}\tag{2}$$

The liquid-drop model parameters are $a_v=15.677$ MeV, $a_s=18.56$ MeV, $a_c=0.717$ MeV, $\kappa=1.79$, and $c_4=1.211$ MeV. $I=(N-Z)/A$ denotes the neutron-proton asymmetry of the fragment. The pairing energy (E_{pair}) and shell-correction energy (E_{sh}) of the fragment are given in [82]. The effective nucleus-nucleus interaction potential between the two fragments can be expressed as

$$\begin{aligned}&V_{CN}(Z_1,N_1,\theta_1,\theta_2,R)\\&=V_C(Z_1,N_1,\theta_1,\theta_2,R)+V_N(Z_1,N_1,\theta_1,\theta_2,R).\end{aligned}\tag{3}$$

The Coulomb potential is given by the Wong formula [83], which accounts for the effects of deformation and orientation of the two fragments, as follows:

$$\begin{aligned}&V_C(Z_1,N_1,\theta_1,\theta_2,R)\\&=\frac{Z_1Z_2e^2}{R}+\left(\frac{9}{20\pi}\right)^{1/2}\left(\frac{Z_1Z_2e^2}{R^3}\right)\\&\times\sum_{i=1}^{2}R_i^2\beta_i^{(i)}P_2(\cos\theta_i)+\left(\frac{3}{7\pi}\right)\left(\frac{Z_1Z_2e^2}{R^3}\right)\\&\times\sum_{i=1}^{2}R_i^2\left[\beta_i^{(i)}P_2(\cos\theta_i)\right]^2.\end{aligned}\tag{4}$$

Here, R denotes the center-to-center distance between the two nuclei, R_i denotes the nuclear radius of fragment i, and the nuclear potential term is evaluated using a double-folding potential [84].

$$\begin{aligned}V_N(Z_1,N_1,\theta_1,\theta_2,R)=C_0\Bigg\{&\frac{F_{\rm in}-F_{\rm ex}}{\rho_0}\Bigg[\int\rho_1^2(\mathbf{r})\rho_2(\mathbf{r}-\mathbf{R})\,d\mathbf{r}\\&+\int\rho_1(\mathbf{r})\rho_2^2(\mathbf{r}-\mathbf{R})\,d\mathbf{r}\Bigg]+F_{\rm ex}\int\rho_1(\mathbf{r})\rho_2(\mathbf{r}-\mathbf{R})\,d\mathbf{r}\Bigg\},\end{aligned}$$

with

$$\begin{aligned}F_{\rm in}&=f_{\rm in}+f'_{\rm in}\frac{N_1-Z_1}{A_1}\frac{N_2-Z_2}{A_2},\\F_{\rm ex}&=f_{\rm ex}+f'_{\rm ex}\frac{N_1-Z_1}{A_1}\frac{N_2-Z_2}{A_2}.\end{aligned}\tag{5}$$

For the constant $C_0=300$ MeV fm^3, the recommended amplitude values in Ref. [85] are $f_{in}=0.09$, $f_{ex}=-2.59$, $f'_{in}=0.42$, and $f'_{ex}=0.5$. ρ_0 denotes the average nuclear density at the center of the composite system, while $\rho_1(\mathbf{r})$ and $\rho_2(\mathbf{r}-\mathbf{R})$ represent the density distributions of the two nuclei.

In the DNS model, the state of a dinuclear system can be described by macroscopic collective variables (such as the proton number Z_1 and neutron number N_1). The probability distribution $P(Z_1,N_1,E_1,\theta_1,\theta_2,t)$ in this macroscopic collective-variable representation is obtained primarily by solving the two-dimensional master equation, which characterizes transition probabilities and quasi-fission throughout the evolution. The master equation is given by:

$$\begin{aligned}&\frac{dP(Z_1,N_1,E_1,\theta_1,\theta_2,t)}{dt}\\&=\sum_{Z'_1}W_{Z_1,N_1;Z'_1,N_1}(t)\left[d_{Z_1,N_1}P(Z'_1,N_1,E_1,\theta_1,\theta_2,t)\right.\\&\left.-d_{Z'_1,N_1}P(Z_1,N_1,E_1,\theta_1,\theta_2,t)\right]\\&+\sum_{N'_1}W_{Z_1,N_1;Z_1,N'_1}(t)\left[d_{Z_1,N_1}P(Z_1,N'_1,E_1,\theta_1,\theta_2,t)\right.\\&\left.-d_{Z_1,N'_1}P(Z_1,N_1,E_1,\theta_1,\theta_2,t)\right]\\&-\{\Lambda_{\rm qf}[\Theta(t)]+\Lambda_{\rm fis}[\Theta(t)]\}P(Z_1,N_1,E_1,\theta_1,\theta_2,t),\end{aligned}\tag{6}$$

$W_{Z_1,N_1;Z'_1,N_1}(t)$ and $W_{Z_1,N_1;Z_1,N'_1}(t)$ are the average transition probabilities at time t for transitions from (Z_1,N_1) to (Z'_1,N_1) and from (Z_1,N_1) to (Z_1,N'_1), respectively. The microscopic dimension d_{Z_1,N_1} denotes the number of microscopic states of the fragments corresponding to the macroscopic state (Z_1,N_1,E_1). The dissipation of relative kinetic energy leads to the local excitation energy E_1 of the composite system. $\Lambda_{\rm qf}$ and $\Lambda_{\rm fis}$ denote the quasi-fission and fission rates of the dinuclear system, respectively, as detailed in Ref. [84]. As an example, consider the average proton transition probability $W_{Z_1,N_1;Z'_1,N_1}(t)$:

$$
\begin{aligned}
&W_{Z_1,N_1;Z_1',N_1}(t)\\
&=\frac{\tau_{\rm mem}[Z_1,N_1,E_1(Z_1,N_1);Z_1',N_1,E_1(Z_1',N_1)]}{d_{Z_1,N_1}d_{Z_1',N_1}\hbar^2}\\
&\times\sum_{ii'}\left|\langle Z_1',N_1,E_1(Z_1',N_1),\right.\\
&\left.i'|V(t)|Z_1,N_1,E_1(Z_1,N_1),i\rangle\right|^2.
\end{aligned}
\tag{7}
$$

It is assumed that only one nucleon is transferred at each step, namely $Z_1' = Z_1 \pm 1$ or $N_1' = N_1 \pm 1$. The memory time $\tau_{\rm mem}$ has the following form:

$$
\begin{aligned}
&\tau_{\rm mem}(Z_1,N_1,E_1;Z_1',N_1,E_1';t)\\
&=\hbar\left[\frac{2\pi}{\sum_{KK'}(V_{KK'}V^*_{KK'})}\right]^{1/2}
\end{aligned}
\tag{8}
$$

Further details on $\tau_{\rm mem}$ can be found in Ref. [86].

The local excitation energy E_1 of the DNS is given by:

$$
\begin{aligned}
E_1(Z_1,N_1) = E_{\rm diss} - \frac{M^2}{2\zeta_{\rm int}} - [U(Z_1,N_1,\theta_1,\theta_2)\\
- U(Z_p,N_p,\theta_1,\theta_2)],
\end{aligned}
\tag{9}
$$

In this expression, M and $\zeta_{\rm int}$ denote, respectively, the intrinsic angular momentum transferred to the DNS and the intrinsic moment of inertia. E_{diss} represents the energy dissipated into the DNS from the kinetic energy of the relative motion, which can be determined by

$$
\begin{aligned}
E_{\rm diss}(t) = E_{\rm c.m.} - V_{\rm CN}(Z_p,N_p,R_{\rm cont})\\
- \frac{\langle J(t)\rangle^2}{2\zeta_{\rm rel}} - E_{\rm rad}(t),
\end{aligned}
\tag{10}
$$

The interaction potential corresponding to the entrance channel is denoted by $V_{\rm CN}(Z_p,N_p,R_{\rm cont})$. The dissipation of the relative angular momentum, $\langle J(t)\rangle$, can be expressed as $\langle J(t)\rangle = J_{st} + (J - J_{st})\exp(-t/\tau_J)$, where J_{st} represents the angular momentum in the sticking limit. The radial energy at time t is given by $E_{\rm rad}(t) = E_{\rm rad}(t=0)\exp(-t/\tau_{\rm R})$, where $\tau_{\rm R}$ denotes the relaxation time of the radial kinetic energy.

The evolution of the mass-distribution probability ends when the time reaches the interaction time. The interaction time is calculated using the deflection function method:

$$
\tau_{\rm int}(l_i,\Delta\theta) = \frac{\Delta\theta}{\hbar l_i}\zeta_{\rm tol} + \frac{1}{\kappa}\ln\frac{l_f}{l_i}.
\tag{11}
$$

Here, $\Delta\theta$ denotes the rotation angle of the DNS; l_i and l_f represent the initial and final angular momenta, respectively; $\zeta_{\rm tol}$ is the total rotational inertia; and κ is the relaxation constant.

The production cross section for the initial fragment with proton number Z_1 and neutron number N_1 is given by the following equation:

$$
\begin{aligned}
\sigma_{\rm pr}(Z_1,N_1,E_{\rm c.m.}) = \frac{\pi\hbar^2}{2\mu E_{\rm c.m.}}\sum_J(2J+1)\\
\times[P(Z_1,N_1,E_1,t=\tau_{\rm int})].
\end{aligned}
\tag{12}
$$

In the equation above, μ denotes the reduced mass of the system, and $P(Z_1,N_1,E_1,t=\tau_{\rm int})$ represents the probability distribution of fragments at time $t=\tau_{\rm int}$.

The statistical model Gemini++ is used to describe the subsequent de-excitation of excited fragments [79, 80]. This model fully accounts for the evaporation of light charged particles, symmetric fission, and all possible evaporation channels. Furthermore, the Hauser-Feshbach theory is employed to describe the evaporation of light particles. For the emission of heavier fragments and the asymmetric fission of heavy systems, the Gemini++ model not only adopts the Moretto formalism but also incorporates structural evolution based on the Bohr-Wheeler formalism.

III. RESULTS AND DISCUSSION

To assess the reliability of the DNS model combined with the statistical decay model GEMINI++ in describing the generation mechanism of heavy system fragments, we investigate the production cross sections of nuclei with Z = 97-100 in the multinucleon transfer reaction ^{48}Ca+^{248}Cm at $E_{c.m.}$=260 MeV, as shown in Fig. 1. The black solid lines, blue dashed lines, olive short-dotted lines, and orange dash-dotted lines represent the calculated results for tip-to-tip, side-to-side, tip-to-side, and side-to-tip configurations, respectively. The red solid circles denote the experimental values, taken from Ref. [87]. The tip-to-tip configuration shows the best agreement with the experimental data, closely reproducing the peak position and width and the declining trend on the neutron-rich side. This indicates that the tip-to-tip configuration is most favorable for nucleon transfer. The side-to-side configuration significantly underestimates the experimental yields, with even greater deviations on the neutron-rich side, suggesting that it leads to a higher potential barrier and a shorter interaction time, thereby severely suppressing the calculated cross sections. The tip-to-side and side-to-tip configurations lie between these extremes but still fall below the experimental data overall, indicating that asymmetric orientations contribute to some extent but are insufficient to fully reproduce the measured cross sections. These comparisons demon-

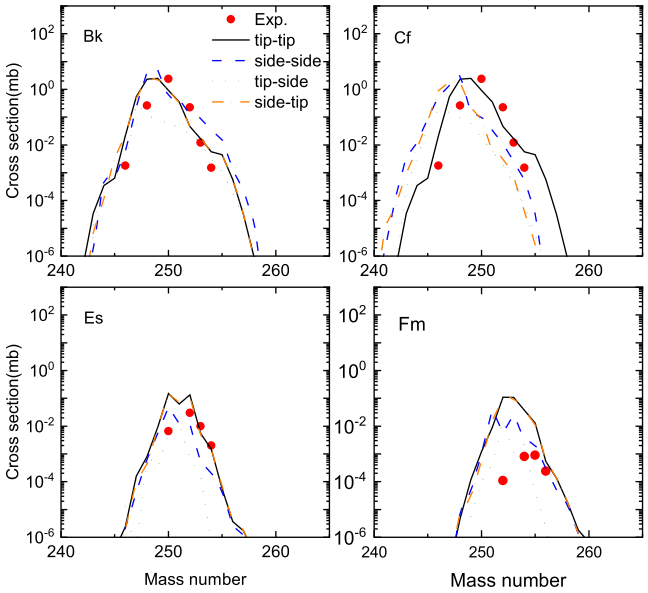

Fig. 1. (Color online) Isotopic cross sections for secondary fragments with Z =97 to 100 of the tip-to-tip (black solid lines),side-to-side (blue dashed lines), tip-to-side (olive short dotted lines), and side-to-tip (orange dash-dotted lines) configurations in the reaction ^{48}Ca+^{248}Cm at $E_{c.m.}$=260 MeV. The red solid circles indicate experimental values, which are derived from Ref. [87].

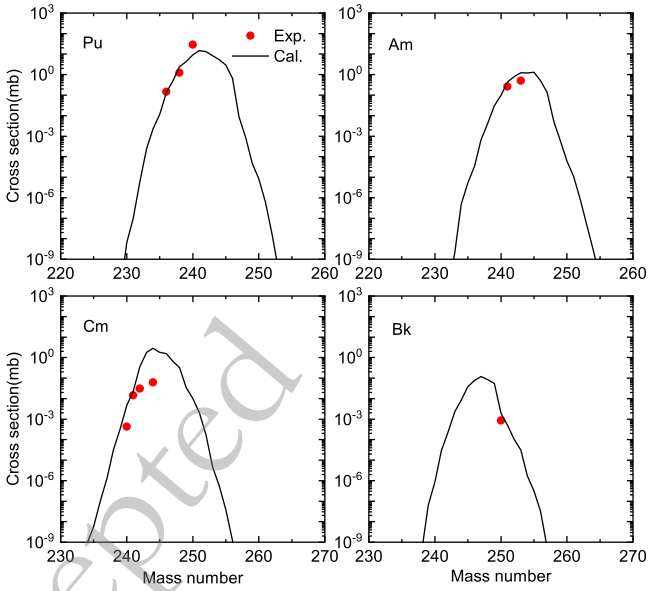

Fig. 2. (Color online) Isotopic cross sections for secondary fragments with Z =94 to 97 in the reactioin of ^{238}U+^{238}U at $E_{c.m.}$=825 MeV. The red solid circles represent experimental data, which are obtained from Ref. [29].

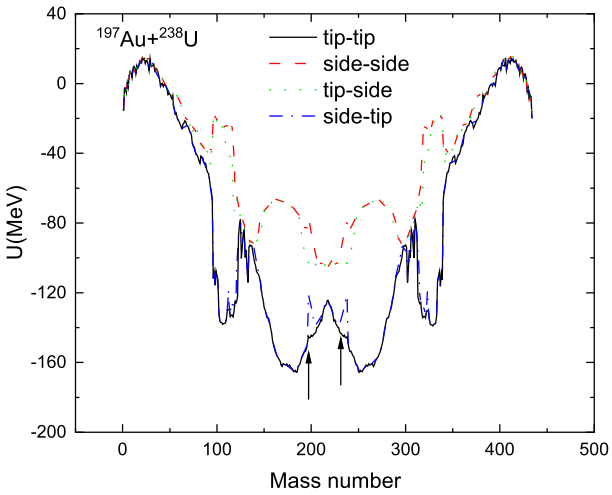

Fig. 3. (Color online) The driving potential of the tip-to-tip (black solid line), side-to-side (red dashed line), tip-to-side (olive short dotted line), and side-to-tip (blue dash-dotted line) configurations in the reaction of ^{197}Au+^{238}U.

strate that, in deformed heavy nuclear systems, collision orientation must be considered to accurately describe multinucleon transfer reactions, and that the tip-to-tip configuration plays a key role in achieving consistency between theoretical calculations and experimental results.

Because this work focuses on reactions with uranium targets, the production cross sections of nuclei with Z = 94-97 in the reaction ^{238}U+^{238}U at $E_{c.m.}$=825 MeV are shown in Fig. 2 to further validate the model. The experimental data, taken from Ref. [29] and shown as red solid circles, agree well with the calculated results (see Fig. 2), further demonstrating the model's reliability for uranium-target reactions.

To investigate how collision orientation influences nucleon transfer in multinucleon transfer reactions, we calculate the differences in driving potentials for various orientations. The driving potential as a function of fragment mass number for four orientations in the ^{197}Au+^{238}U reaction is shown in Fig. 3. The tip-to-tip configuration (black solid line) exhibits a pronounced potential valley in the heavy-mass region (mass numbers around 200-250) and yields the lowest driving potential, indicating that it is most favorable for nucleon transfer from the light to the heavy nucleus and provides an efficient pathway to neutron-rich heavy products. The side-to-side configuration (red dashed line) exhibits the highest driving potential, rising markedly in the heavy-mass region; characterized by a high Coulomb barrier and weak nuclear attraction, it is unfavorable for deep nucleon transfer. The tip-to-side (olive dotted line) and side-to-tip (blue dash-dotted line) configurations yield driving potentials that fall between these extremes and are closer to the tip-to-tip case, indicating that asymmetric orientations still permit a non-negligible transfer probability. Overall, the depth and valley structure of the driving potential are key determinants of the ease of nucleon transfer, making the tip-to-tip collision the optimal geometric condition in experiments because of its lowest driving potential.

The standard quasifission process involves the trans-

fer of nucleons from heavier to lighter nuclei. In more symmetric reaction systems, the "inverse" quasifission process enables transfer from lighter to heavier nuclei, thereby increasing system asymmetry. The "inverse" quasifission mechanism is closely related to the deformation, orientation, and shell structure of the entrance channel. More detailed theoretical calculations will facilitate the design of experiments on actinide projectile-target transfer reactions. "Inverse" quasifission processes are crucial for producing neutron-rich transuranium nuclides with Z=93-101. To identify optimal projectile-target combinations, we investigate multinucleon transfer induced by stable beams of ^{197}Au, ^{186}W, and ^{232}Th on the actinide target ^{238}U. Notably, the three-dimensional potential-energy surface plays a pivotal role in determining fragment-formation probabilities during nucleon transfer.

The three-dimensional PES critically influences the calculation of fragment-formation probabilities in the nucleon-transfer process. Fig. 4 illustrates the potential-energy surface distributions as functions of the proton number Z and neutron number N of the fragments for three reaction systems: ^{197}Au+^{238}U, ^{186}W+^{238}U, and ^{232}Th+^{238}U. The black solid lines indicate the minimum-value paths of the PES, and the open circles denote the injection points. For the ^{197}Au+^{238}U and ^{186}W+^{238}U systems, the injection points do not lie at the bottom of the potential valley but are located in regions of higher energy. Moreover, the PES exhibits distinct double-valley structures around $Z = 64, 100$ and $N = 100, 152, 162$, a hallmark of the "inverse" quasifission process driven by shell effects. This implies that nucleons tend to transfer from the light nuclei (Au and W) to the heavy nucleus (U), thereby favoring the production of neutron-rich heavy nuclides. In contrast, the injection points of the ^{232}Th+^{238}U system lie precisely on the minimum-value path, corresponding to a normal quasifission process. The depth of the valleys in the PES and the relative positions of the injection points directly determine the ease of nucleon transfer and the distributions of reaction products, providing a crucial theoretical basis for selecting optimal projectile-target combinations and predicting the yields of neutron-rich nuclides.

To further investigate the direction of nucleon transfer in the "inverse" quasifission process, we analyze the driving potential as a function of the fragment mass number for collisions of ^{197}Au+^{238}U (black solid line), ^{186}W+^{238}U (red dashed line), and ^{232}Th+^{238}U (blue dash-dotted line) in Fig. 5. Fig. 5 demonstrates that the driving potential of ^{186}W+^{238}U is the highest among the three reaction systems. It can be observed that the driving potentials of the ^{197}Au+^{238}U and ^{186}W+^{238}U systems exhibit a decreasing trend in the heavy-mass region, indicating that nucleons tend to transfer from the lighter to the heavier nucleus, a typical feature of the "inverse" quasifission process. In contrast, the driving potential of the

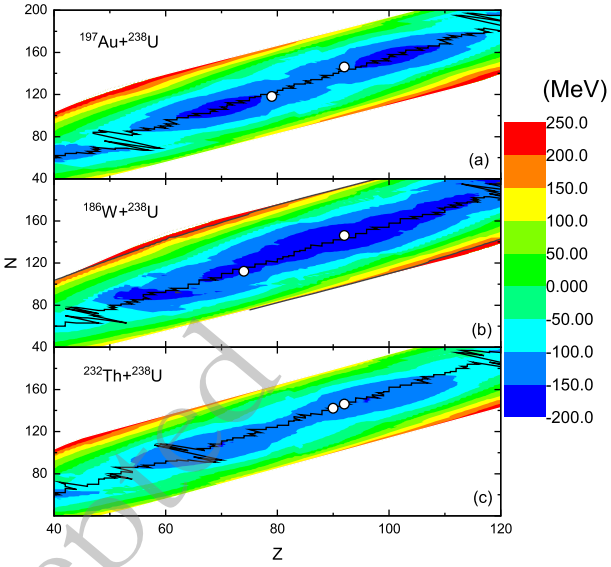

Fig. 4. (Color online) The potential-energy surface (PES) as a function of Z and N of the fragments in collisions of (a) ^{197}Au+^{238}U, (b) ^{186}W+^{238}U, and (c) ^{232}Th+^{238}U. The black solid lines indicate the minimum value in the PES. The open circles represent the injection points.

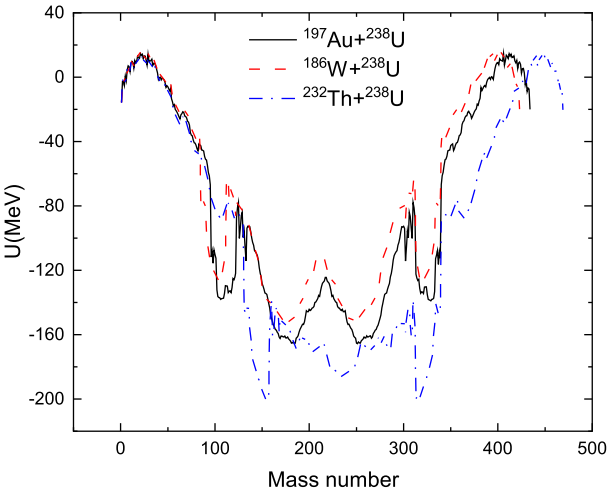

Fig. 5. (Color online) The driving potentials in the reactions of ^{197}Au+^{238}U(black solid line), ^{186}W+^{238}U(red dashed line), and ^{232}Th+^{238}U(blue dash-dotted line).

^{232}Th+^{238}U system is relatively flat near the injection points, corresponding to a normal quasifission process. Fig. 6 focuses on the local driving potential of the ^{197}Au+^{238}U reaction, where downward arrows mark the incident points and upward arrows indicate the positions of subshells (near Z=64,100 and N=100,152,162). It can be seen that distinct potential valleys appear in the driving potential around these subshell closures. These valleys, induced by shell effects, allow the reaction system to evolve more easily along the valley floor, thereby enhancing the production yields of neutron-rich heavy nuclides. Fig. 5 and Fig. 6 reveal that by selecting an appro-

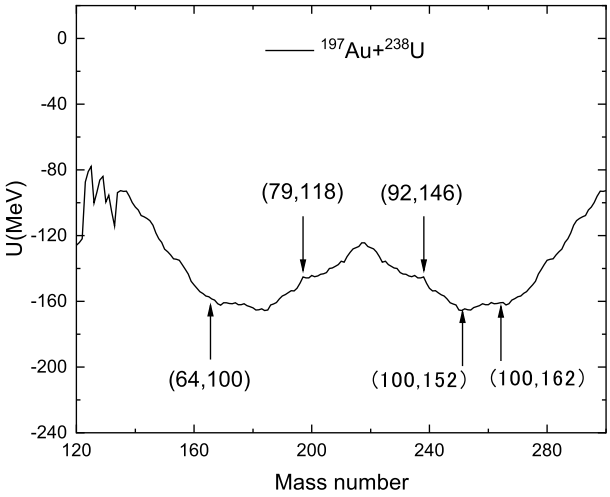

Fig. 6. (Color online) The local driving potential of the reaction of ^{197}Au+^{238}U. The downward arrows indicate the positions of the incident points, while the upward arrows denote the subshell near the incident points.

priate projectile-target combination (such as ^{197}Au+^{238}U) and utilizing the potential valleys induced by shell effects along with the "inverse" quasifission mechanism, the production cross sections of neutron-rich heavy nuclei in multinucleon transfer reactions can be significantly enhanced, providing theoretical guidance for the experimental synthesis of new nuclides.

Multinucleon transfer reactions with uranium targets have been extensively investigated for many years. As the heaviest naturally occurring element, uranium possesses a high N/Z ratio and significant quadrupole deformation, making it an ideal "neutron-rich reservoir". At near-barrier energies, collisions between a uranium target and deformed projectiles can readily induce deep nucleon transfer, producing target-like fragments with atomic numbers Z near 92. However, the cross sections are generally low, placing stringent demands on the predictive accuracy of theoretical models. Refs. [55, 88] suggest that an incident energy of $1.10V_B$ is suitable for studying entrance-channel effects in multinucleon transfer reactions. V_B denotes the Bass interaction barrier [89]. Accordingly, this section uses a center-of-mass energy of $1.10V_B$ to analyze isotope production cross sections in target-like fragments with atomic numbers ranging from 93 to 101.

Fig. 7 shows the final production cross sections of target-like fragments with atomic numbers Z=93-101 for three reaction systems. The black solid lines, red dashed

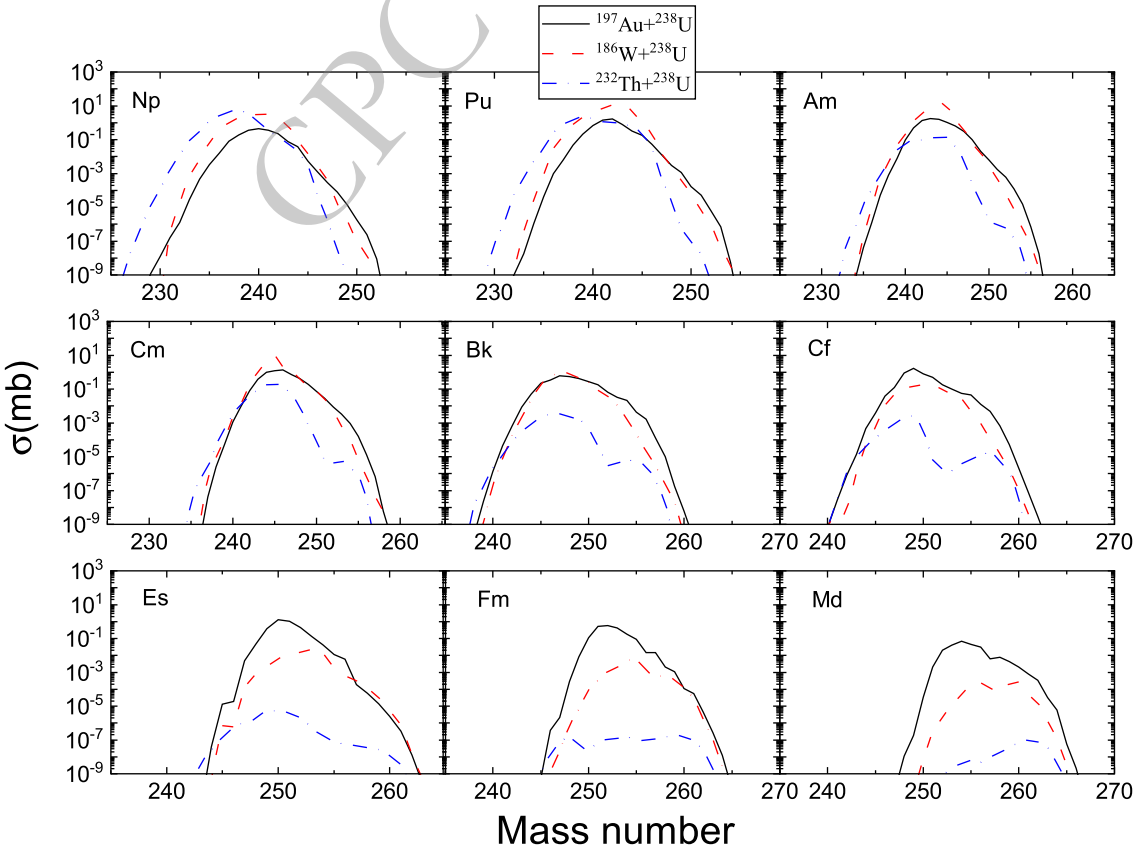

Fig. 7. (Color online) The final isotopic production cross sections of target-like fragments with Z=93-101 at the incident energy of $E_{c.m.}$=$1.10V_B$. The black solid lines, red dashed lines, and blue dash-dotted lines represent the transfer reactions ^{197}Au+^{238}U, ^{186}W+^{238}U, and ^{232}Th+^{238}U, respectively. V_B denotes the Bass interaction barrier[89].

lines, and blue dash-dotted lines represent the transfer reaction ^{197}Au+^{238}U, ^{186}W+^{238}U, and ^{232}Th+^{238}U, respectively. The V_B values for the multinucleon transfer reaction systems ^{197}Au+^{238}U, ^{186}W+^{238}U, and ^{232}Th+^{238}U are 671.0,630.8, and 748.9 MeV, respectively. It can be observed that the cross sections for all three systems decrease with increasing proton number, but the extent of the decrease and the absolute magnitudes differ significantly. Among them, the ^{197}Au+^{238}U system exhibits higher cross sections than the other two for nearly all isotopes. This is consistent with the conclusion drawn from the earlier driving potential analysis, where this system showed the deepest potential valley and the smallest potential need to overcome in the transfer process, confirming the enhancement effect of the "inverse" quasifission mechanism on the production of neutron-rich nuclides. The system ^{186}W+^{238}U ranks second, while the ^{232}Th+^{238}U system has the lowest cross sections, dropping sharply below the detectable limit for $Z \geq 98$. These quantitative results indicate that, for combinations of a uranium target with lighter deformed projectiles, the nucleon transfer path driven by shell effects is more favorable for producing neutron-rich target-like fragments with high atomic numbers, providing a clear numerical basis for selecting optimal projectile-target combinations in experiments. Compared to the reaction systems ^{186}W+^{238}U and ^{232}Th+^{238}U, the multinucleon transfer reaction ^{197}Au+^{238}U is the optimal projectile-target combination for generating new neutron isotopes with atomic numbers Z=93-101.

The ^{197}Au+^{238}U transition reaction exhibits an "inverse" quasi-fission process, granting the reaction system a significant advantage in producing heavy neutron isotopes with Z ranging from 93 to 101 as studied above. To further investigate the optimal incident energy for this reaction, Fig. 8 demonstrates the final isotope production cross sections of target-like fragments in the ^{197}Au+^{238}U transition reaction at different incident energies. The black solid lines, red dashed lines, and blue dash-dotted lines represent the incident energies in the center-of-mass system of $1.05V_B$,$1.10V_B$, and $1.15V_B$, respectively. The blank symbols indicate the unknown new neutron-rich nuclei. It can be observed that the production cross sections for all three energies decrease with increasing proton number, but the energy dependence exhibits distinct regional characteristics. In the Z=93-98 region, the production cross sections increase with higher incident energy, with the highest values occurring at $1.15V_B$, indicating that a higher energy facilitates overcoming the poten-

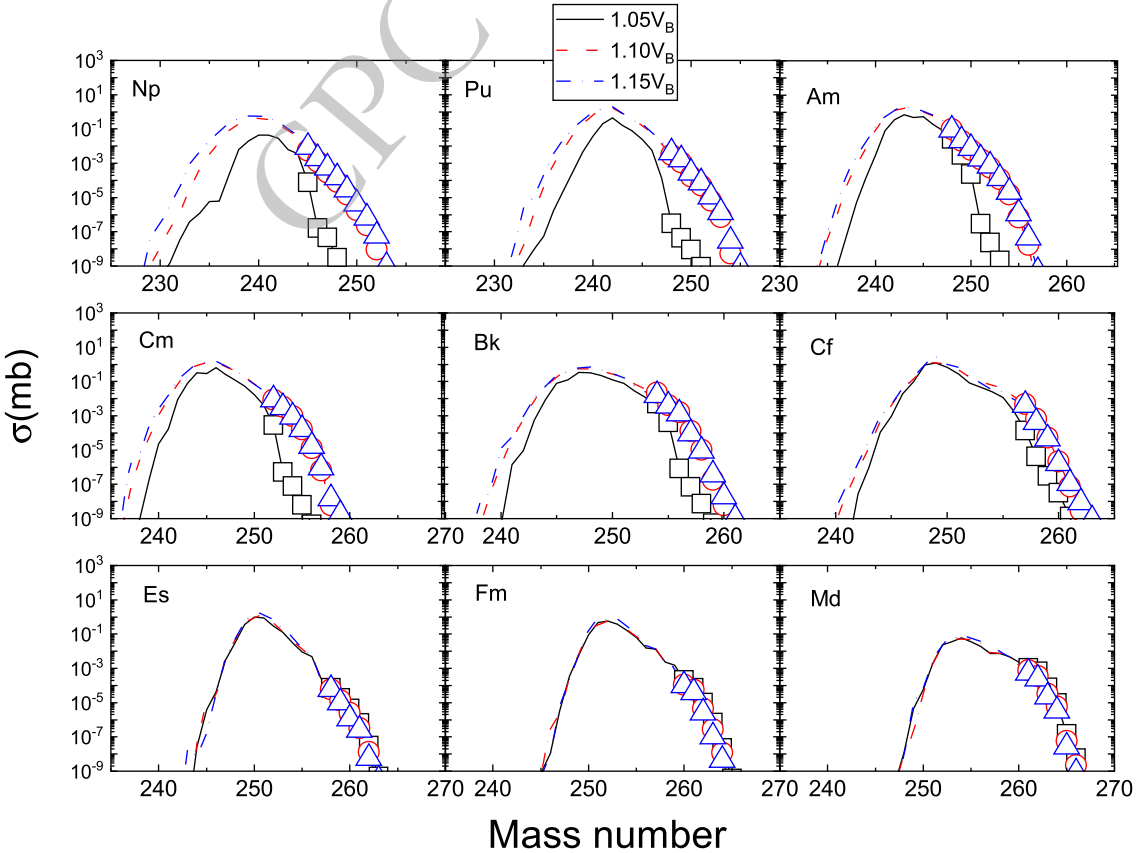

Fig. 8. (Color online) The final isotopic production cross sections of target-like fragments with $Z = 93 - 101$ in the transfer reaction ^{197}Au+^{238}U at $E_{c.m.}$=$1.05V_B$(black solid lines), $1.10V_B$ (red dashed lines), and $1.15V_B$ (blue dash-dotted lines), respectively. The blank symbols indicate the unknown neutron-rich nuclei.

tial barrier and drives more nucleon transfer from the projectile to the target. In contrast, in the Z=99-101 region, the differences in production cross sections among the three energies become smaller, with $1.05V_B$ showing a slight advantage. This reflects the effect of enhanced fission competition at higher excitation energies, which reduces the survival probability of heavy nuclei. One can see that a total of 61 unknown neutron-rich nuclei would expect to be produced with cross sections greater than 1 pb, filling the gap in the region of transuranium. The calculated production cross sections of ^{245,246,247,248,249,250,251,252}Np are 8.49μb, 1.9μb, 0.52μb, 0.14μb, 0.03μb, $4.16\times10^{-3}\mu$b, $6.26\times10^{-4}\mu$b, and $5.58\times10^{-5}\mu$b, respectively. For ^{248,249,250,251,252,253,254}Pu, they are 4.18μb, 1.62μb, 0.26μb, 0.07μb, 0.01μb, $1.33\times10^{-3}\mu$b, and $2.90\times10^{-5}\mu$b, respectively. The predicted production cross sections of ^{248,249,250,251,252,253,254,255,256}Am are 101.73μb,22.47μb, 7.7μb, 1.91μb, 0.72μb, 0.14μb, 0.02μb, $1.18\times10^{-3}\mu$b, and $4.74\times10^{-5}\mu$b, respectively. ^{252,253,254,255,256,257,258,259}Cm are 8.82μb, 3.01μb,0.85μb, 0.16μb, 0.02μb, $9.13\times10^{-4}\mu$b, $1.45\times10^{-5}\mu$b, and $1.70\times10^{-4}\mu$b, respectively. The production cross sections of ^{254,255,256,257,258,259,260}Bk are 21.75μb, 4.23μb, 1.63μb, 0.13μb, 0.01μb, $3.66\times10^{-4}\mu$b, and $1.85\times10^{-5}\mu$b, respectively. ^{257,258,259,260,261,262}Cf are 4.91μb, 0.67μb, 0.05μb, $2.14\times10^{-3}\mu$b, $1.13\times10^{-4}\mu$b, and $8.59\times10^{-6}\mu$b, respectively. ^{258,259,260,261,262}Es are 0.07μb, 0.02μb, $4.47\times10^{-3}\mu$b, $6.49\times10^{-4}\mu$b, and $3.05\times10^{-5}\mu$b, respectively. The calculated production cross sections of ^{260,261,262,263,264}Fm are 0.21μb, 0.07μb, $9.66\times10^{-3}\mu$b, $6.9\times10^{-4}\mu$b, and $2.25\times10^{-5}\mu$b, respectively. For ^{261,262,263,264,265,266}Md, they are 1.07μb, 0.65μb, 0.08μb, $9.31\times10^{-3}\mu$b, $1.48\times10^{-4}\mu$b, and $5.79\times10^{-6}\mu$b, respectively. These results quantitatively reveal the dual effect of incident energy on the production of multinucleon transfer reactions and provide important guidance for selecting the optimal energy.

Fig. 9 presents the interaction time as a function of the impact parameter for the reaction system ^{197}Au+^{238}U at three incident energies. The black solid lines, red dashed lines, and blue dash-dotted lines represent the incident energies in the center-of-mass system of $1.05V_B$, $1.10V_B$, and $1.15V_B$, respectively. For a given incident energy, the interaction time decreases monotonically with increasing impact parameter. When the impact parameter approaches or exceeds a certain critical value, the interaction time tends to zero, indicating that nucleon transfer hardly occurs in peripheral collisions. Moreover, the interaction time exhibits a clear positive correlation with the incident energy: the higher the incident energy, the longer the interaction time for the same impact parameter, and the temporal spread in the large impact parameter region also becomes more pronounced. This is mainly because a higher incident energy provides the system with more relative kinetic energy, allowing the two nuclei to maintain longer contact and evolution time after overcoming the potential barrier, thereby facilitating deep nucleon transfer. These results, from a dynamic perspective, explain why higher incident energies lead to higher produciton cross sections in the Z=93-98 region, and, together with the effect of fission competition, also reveal the complex energy dependence of production cross sections in the medium to heavy mass region.

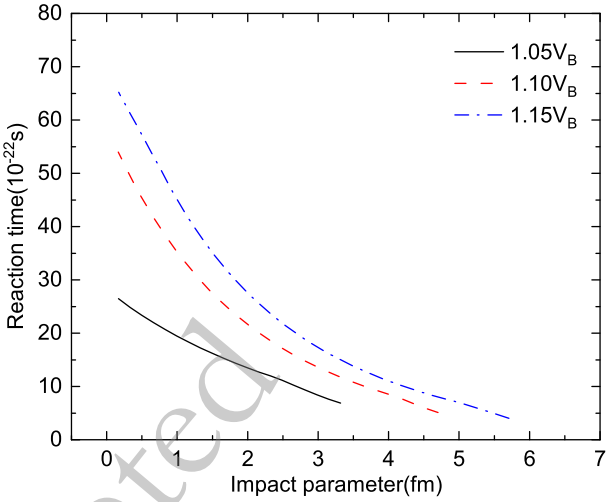

Fig. 9. (Color online) The calculated interaction time as a function of the impact parameter for the reaction system ^{197}Au+^{238}U at three different incident energies. The black solid, red dashed, and blue dotted lines represent the incident energies at $E_{c.m.}$=$1.05V_B$, $1.10V_B$, and $1.15V_B$, respectively.

IV. SUMMARY

By combining the DNS model with the GEMINI++ de-excitation code, this work systematically investigates the theoretical mechanisms for synthesizing neutron-rich heavy nuclei in multinucleon transfer reactions with uranium as the target, considering aspects such as collision orientation, shell effects, projectile-target combinations, and incident energy. Regarding the effect of collision orientation, based on calculations and experimental comparisons for the ^{48}Ca+^{248}Cm reaction, the tip-to-tip configuration shows the best agreement with experimental data. It exhibits the lowest driving potential and the most pronounced potential valley in the heavy mass region, making it the most favorable for nucleon transfer from the light nucleus to the heavy nucleus. In contrast, the side-to-side configuration significantly underestimates the production cross sections, while the tip-to-side and side-to-tip configurations fall between these extremes, confirming that collision orientations must be considered in deformed heavy nuclear systems to accurately describe multinucleon transfer reactions. The model can also well reproduce the transfer reaction cross sections of nuclei with Z =94 to 97 in the ^{238}U+^{238}U reaction.

Regarding shell effects and the "inverse" quasifission mechanism, potential-energy surface analysis reveals that the injection points of the ^{197}Au+^{238}U and ^{186}W+^{238}U systems deviate from the potential valley bottom and exhibit distinct double-valley structures near Z=64,100 and N=100,152,162, characteristic of the "inverse" quasifission process, whereas the injection points of the ^{232}Th+^{238}U system located at the valley bottom, corresponding to a normal quasifission process. Comparisons of the driving potentials further confirm this classification, and in the ^{197}Au+^{238}U reaction, the positions of these subshells correspond to pronounced potential valleys, thereby enhancing the yields of neutron-rich heavy nuclides.

The final production cross sections of target-like fragments with Z=93-101 for the three systems are calculated at $E_{c.m.}$=1.10V_B. It is found that the production cross sections of the ^{197}Au+^{238}U system are significantly higher than those of the ^{186}W+^{238}U and ^{232}Th+^{238}U systems, especially in the Z=93-98 region, confirming that this combination is the optimal choice for synthesizing neutron-rich actinide nuclei. Further analysis of the incident energy effect on the reaction ^{197}Au+^{238}U shows that for Z=93-98, the production cross sections increase with incident energy, peaking at 1.15V_B, while for Z=99-101, the lower energy yields slightly higher cross sections, reflecting the trade-off where higher excitation energies enhance fission competition and reduce the survival probability of heavy nuclei. Concurrently, calculations of the interaction time confirm that higher incident energies lead to longer contact times between the nuclei, providing a dynamical explanation for deeper nucleon transfer. Based on these analyses, this work predicts the production cross sections for 61 unknown neutron-rich nuclides with cross sections greater than 1 pb, which are relatively higher at 1.05V_B, indicating that lower incident energies are more favorable for synthesizing new neutron-rich nuclides in the superheavy region.

ACKNOWLEDGEMENTS

This work systematically elucidates the mechanisms by which collision orientation, shell effects, projectile-target combinations, and incident energies influence the production cross sections in uranium-target multinucleon transfer reactions, and predicts the cross sections for a number of unknown neutron-rich nuclides, providing important theoretical guidance for future experimental synthesis.

References

[1] S. Hofmann and G. Münzenberg, Rev. Mod. Phys. **72**, 733 (2000)
[2] W. D. Myers and W. J. Swiatecki, Nucl. Phys. **81**, 1 (1966)
[3] T. Otsuka, Physics **4**, 258 (2022)
[4] S. Heinz and H. Devaraja, Eur. Phys. J. A **58**, 114 (2022)
[5] J. J. Cowan, F.-K. Thielemann, and J. W. Truran, Phys. Rep. **208**, 267 (1991)
[6] K. Langanke and M. Wiescher, Repo. Pro. in Phys. **64**, 1657 (2001)
[7] K. E. Gregorich, K. J. Moody, D. Lee, W. K. Kot, R. B. Welch, P. A. Wilmarth, and G. T. Seaborg, Phys. Rev. C **35**, 2117 (1987)
[8] A. Artukh, G. Gridnev, V. Mikheev, and V. Volkov, Nucl. Phys. A **137**, 348 (1969)
[9] G. Gridnev, V. Volkov, and J. Wilczynski, Nucl. Phys. A **142**, 385 (1970)
[10] A. Artukh, V. Avdeichikov, G. Gridnev, V. Mikheev, V. Volkov, and J. Wilczynski, J. Phys. Colloques **32**, C6 (1971)
[11] A. Artukh, G. Gridnev, V. Mikheev, V. Volkov, and J. Wilczynski, Nucl. Phys. A **211**, 299 (1973)
[12] J. Galin, D. Guerreau, M. Lefort, J. Peter, X. Tarrago, and R. Basile, Nucl. Phys. A **159**, 461 (1970)
[13] F. Hanappe, M. Lefort, C. Ngô, J. Péter, and B. Tamain, Phys. Rev. Lett. **32**, 738 (1974)
[14] J. V. Kratz, A. E. Norris, and G. T. Seaborg, Phys. Rev. Lett. **33**, 502 (1974)
[15] J. V. Kartz, J. O. Liljenzin, A. E. Norris, and G. T. Seaborg, Phys. Rev. C **13**, 2347 (1976)
[16] R. J. Otto, M. M. Fowler, D. Lee, and G. T. Seaborg, Phys. Rev. Lett. **36**, 135 (1976)
[17] K. L. Gippert, E. Runte, W. D. Schmidt-Ott, P. Tidemand-Petersson, N. Kaffrell, P. Peuser, R. Kirchner, O. Klepper, W. Kurcewicz, P. Larsson, E. Roeckl, D. Schardt, and K. Rykaczewski, Nucl. Phys. A **453**, 1 (1986)
[18] K. D. Hildenbrand, H. Freiesleben, F. Pühlhofer, W. F. W. Schneider, R. Bock, D. v. Harrach, and H. J. Specht, Phys. Rev. Lett. **39**, 1065 (1977)
[19] M. Schädel, J. V. Kratz, H. Ahrens, W. Brüchle, G. Franz, H. Gäggeler, I. Warnecke, G. Wirth, G. Herrmann, N. Trautmann, and M. Weis, Phys. Rev. Lett. **41**, 469 (1978)
[20] J. Kratz, W. Loveland, and K. Moody, Nucl. Phys. A **944**, 117 (2015)
[21] J. S. Barrett, W. Loveland, R. Yanez, S. Zhu, A. D. Ayangeakaa, M. P. Carpenter, J. P. Greene, R. V. F. Janssens, T. Lauritsen, E. A. McCutchan, A. A. Sonzogni, C. J. Chiara, J. L. Harker, and W. B. Walters, Phys. Rev. C **91**, 064615 (2015)
[22] R. Yanez and W. Loveland, Phys. Rev. C **91**, 044608 (2015)
[23] T. Welsh, W. Loveland, R. Yanez, J. Barrett, E. McCutchan, A. Sonzogni, T. Johnson, S. Zhu, J. Greene, A. Ayangeakaa, M. Carpenter, T. Lauritsen, J. Harker, W. Walters, B. Amro, and P. Copp, Phys. Lett. B **771**, 119 (2017)
[24] V. Desai, W. Loveland, R. Yanez, G. Lane, S. Zhu, A. Ayangekaa, J. Greene, F. G. Kondev, R. Janssens, and P. Copp, Eur. Phys. J. A **56**, 150 (2020)
[25] V. V. Desai, A. Pica, W. Loveland, J. S. Barrett, E. A. McCutchan, S. Zhu, A. D. Ayangeakaa, M. P. Carpenter, J. P. Greene, T. Lauritsen, R. V. F. Janssens, B. M. S. Amro,

and W. B. Walters, Phys. Rev. C **101**, 034612 (2020)
[26] Y. X. Watanabe, Y. H. Kim, S. C. Jeong, Y. Hirayama, N. Imai, H. Ishiyama, H. S. Jung, H. Miyatake, S. Choi, J. S. Song, E. Clement, G. de France, A. Navin, M. Rejmund, C. Schmitt, G. Pollarolo, L. Corradi, E. Fioretto, D. Montanari, M. Niikura, D. Suzuki, H. Nishibata, and J. Takatsu, Phys. Rev. Lett. **115**, 172503 (2015)
[27] C. Golabek, A. C. C. Villari, S. Heinz, W. Mittig, S. Bhattacharyya, D. Boilley, G. De France, A. Drouart, L. Gaudfefroy, L. Giot, A. Marchix, V. Maslov, M. Morjean, G. Mukherjee, A. Navin, Y. Penionzkevich, F. Rejmund, M. Rejmund, P. Roussel-Chomaz, and C. Stodel, Int. J. Mod. Phys. E **17**, 2235 (2008)
[28] C. Golabek, S. Heinz, W. Mittig, F. Rejmund, A. C. C. Villari, S. Bhattacharyva, D. Boilley, G. De France, A. Drouart, L. Gaudefroy, L. Giot, V. Maslov, M. Morjean, G. Mukherjee, Y. Penionzkevich, P. Roussel-Chomaz, and C. Stodel, Eur. Phys. J. A **43**, 251 (2010)
[29] J. V. Kratz, M. Schädel, and H. W. Gäggeler, Phys. Rev. C **88**, 054615 (2013)
[30] M. Barbui, K. Hagel, J. B. Natowitz, A. Bonasera, R. Wada, P. K. Sahu, T. Materna, Z. Chen, L. Quin, G. A. Souliotis, G. Chubaryan, D. Fabris, M. Lunardon, M. Morando, S. Moretto, G. Nebbia, S. Pesente, G. Viesti, F. Bocci, M. Cinausero, V. Rizzi, G. Prete, S. Kowalski, Z. Majka, A. Wieloch, F. D. Becchetti, T. W. O'Donnel, and H. Griffin, J. of Phys.: Conf. Ser. **312**, 082012 (2011)
[31] H. Devaraja, S. Heinz, D. Ackermann, T. Göbel, F. Heßberger, S. Hofmann, J. Maurer, G. Münzenberg, A. Popeko, and A. Yeremin, Eur. Phys. J. A **56**, 224 (2020)
[32] M. E. Gooden, R. C. Malone, T. A. Bredeweg, E. M. Bond, S. W. Finch, C. R. Howell, Krishichayan, A. P. D. Ramirez, J. A. Silano, M. A. Stoyer, A. P. Tonchev, W. Tornow, D. Vieira, and J. B. Wilhelmy, Phys. Rev. C **109**, 044604 (2024)
[33] Y. T. Oganessian, V. K. Utyonkov, M. V. Shumeiko, F. S. Abdullin, G. G. Adamian, S. N. Dmitriev, D. Ibadullayev, M. G. Itkis, N. D. Kovrizhnykh, D. A. Kuznetsov, O. V. Petrushkin, A. V. Podshibiakin, A. N. Polyakov, A. G. Popeko, I. S. Rogov, R. N. Sagaidak, L. Schlattauer, V. D. Shubin, D. I. Solovyev, Y. S. Tsyganov, A. A. Voinov, V. G. Subbotin, N. S. Bublikova, M. G. Voronyuk, A. V. Sabelnikov, A. Y. Bodrov, N. V. Aksenov, A. V. Khalkin, Z. G. Gan, Z. Y. Zhang, M. H. Huang, and H. B. Yang, Phys. Rev. C **109**, 054307 (2024)
[34] N. Wang, Z. Li, and X. Wu, Phys. Rev. C **65**, 064608 (2002)
[35] J. Tian, X. Wu, K. Zhao, Y. Zhang, and Z. Li, Phys. Rev. C **77**, 064603 (2008)
[36] N. Wang, L. Ou, Y. Zhang, and Z. Li, Phys. Rev. C **89**, 064601 (2014)
[37] C. Li, T. Li, X. R. Zhang, J. L. Tian, N. Wang, C. C. Guo, and F. S. Zhang, Phys. Rev. C **110**, 044615 (2024)
[38] K. Zhao, Z. Liu, F. S. Zhang, N. Wang, and J. Z. Duan, Phys. Rev. C **106**, L011602 (2022)
[39] Y. H. Zhang, G. Zhang, J. J. Li, Z. Liu, A. V. Yeremin, and F. S. Zhang, Phys. Rev. C **106**, 014625 (2022)
[40] D. H. Zhang and F. S. Zhang, Sci. Sin.-Phys. Mech. Astron. **55**, 122009 (2025)
[41] Z. Wu and L. Guo, Phys. Rev. C **100**, 014612 (2019)
[42] Z. Gao, Y. Zhang, L. Zhu, Z. Liao, Y. Yang, C. Guo, and J. Su, Phys. Rev. C **109**, L041605 (2024)
[43] X. Jiang and N. Wang, Phys. Rev. C **101**, 014604 (2020)
[44] K. Sekizawa and K. Yabana, Phys. Rev. C **93**, 054616 (2016)
[45] V. Volkov, Phys. Rep. **44**, 93 (1978)
[46] G. Adamian, N. Antonenko, R. Jolos, and W. Scheid, Nucl. Phys. A **619**, 241 (1997)
[47] G. G. Adamian, N. V. Antonenko, S. M. Lukyanov, and Y. E. Penionzhkevich, Phys. Rev. C **78**, 024613 (2008)
[48] G. G. Adamian, N. V. Antonenko, and D. Lacroix, Phys. Rev. C **82**, 064611 (2010)
[49] M. H. Mun, G. G. Adamian, N. V. Antonenko, Y. Oh, and Y. Kim, Phys. Rev. C **89**, 034622 (2014)
[50] M. H. Mun, K. Kwak, G. G. Adamian, and N. V. Antonenko, Phys. Rev. C **99**, 054627 (2019)
[51] M. H. Mun, K. Kwak, G. G. Adamian, and N. V. Antonenko, Phys. Rev. C **101**, 044602 (2020)
[52] J. J. Li, G. Zhang, X. R. Zhang, Y. H. Zhang, Z. Liu, and F. S. Zhang, J. Phys. G: Nucl. Part. Phys. **49**, 025106 (2022)
[53] J. J. Li, N. Tang, Y. H. Zhang, X. R. Zhang, G. Zhang, and F. S. Zhang, Phys. Rev. C **106**, 014606 (2022)
[54] G. Zhang, C. Li, P. W. Wen, J. J. Li, X. X. Xu, B. Li, Z. Liu, and F. S. Zhang, Phys. Rev. C **98**, 014613 (2018)
[55] G. Zhang, C. A. T. Sokhna, Z. Liu, and F. S. Zhang, Phys. Rev. C **100**, 024613 (2019)
[56] X. R. Zhang, G. Zhang, J. J. Li, S. H. Cheng, Z. Liu, and F. S. Zhang, Phys. Rev. C **103**, 024608 (2021)
[57] L. Zhu, J. Su, C. Li, and F. S. Zhang, Phys. Lett. B **829**, 137113 (2022)
[58] L. Zhu and J. Su, Phys. Rev. C **104**, 044606 (2021)
[59] S. Guo, X. Bao, and N. Wang, Phys. Rev. C **103**, 034613 (2021)
[60] X. J. Bao, S. Q. Guo, and P. H. Chen, Phys. Rev. C **105**, 024610 (2022)
[61] L. Zhu, C. Li, J. Su, C.-C. Guo, and W. Hua, Phys. Lett. B **791**, 20 (2019)
[62] X. J. Bao, Phys. Lett. B **833**, 137307 (2022)
[63] P. H. Chen, C. Geng, Z. X. Yang, X. H. Zeng, and Z. Q. Feng, Nucl. Sci. and Tech. **34**, 160 (2023)
[64] J. J. Cai, L. L. Zhou, G. Zhang, L. Q. Li, and F. S. Zhang, Phys. Rev. C **110**, 044602 (2024)
[65] Z. Q. Feng, Phys. Rev. C **108**, L051601 (2023)
[66] D. D. Zhang, D. Vretenar, T. Nikšić, P. W. Zhao, and J. Meng, Phys. Rev. C **109**, 024614 (2024)
[67] B. Li, D. Vretenar, T. Nikšić, D. D. Zhang, P. W. Zhao, and J. Meng, Phys. Rev. C **110**, 034611 (2024)
[68] Y. Zou, M. H. Zhang, M. C. Wang, Y. H. Zhang, and F. S. Zhang, Nucl. Sci. and Tech. **35**, 180 (2024)
[69] V. Saiko and A. Karpov, Eur. Phys. J. A **58**, 41 (2022)
[70] V. V. Saiko and A. V. Karpov, Phys. Rev. C **109**, 064607 (2024)
[71] V. I. Zagrebaev and W. Greiner, Phys. Rev. C **83**, 044618 (2011)
[72] G. A. Souliotis, M. Veselsky, G. Chubarian, L. Trache, A. Keksis, E. Martin, D. V. Shetty, and S. J. Yennello, Phys. Rev. Lett. **91**, 022701 (2003)
[73] F. C. Dai, P. W. Wen, C. J. Lin, J. J. Liu, X. X. Xu, K. L. Wang, H. M. Jia, L. Yang, N. R. Ma, and F. Yang, Phys. Rev. C **109**, 024617 (2024)
[74] S. Ayik, Phys. Lett. B **658**, 174 (2008)
[75] K. Sekizawa and S. Ayik, Phys. Rev. C **102**, 014620 (2020)
[76] S. Ayik, M. Arik, E. C. Karanfil, O. Yilmaz, B. Yilmaz, and A. S. Umar, Phys. Rev. C **104**, 054614 (2021)
[77] S. Ayik, M. Arik, O. Yilmaz, B. Yilmaz, and A. S. Umar, Phys. Rev. C **107**, 014609 (2023)

[78] S. Ayik, M. Arik, O. Yilmaz, and A. S. Umar, Eur. Phys. J. A **62**, 51 (2026)
[79] R. J. Charity, Phys. Rev. C **82**, 014610 (2010)
[80] D. Mancusi, R. J. Charity, and J. Cugnon, Phys. Rev. C **82**, 044610 (2010)
[81] G. Adamian, N. Antonenko, W. Scheid, and V. Volkov, Nuclear Physics A **627**, 361 (1997)
[82] P. Moller, J. Nix, W. Myers, and W. Swiatecki, Atomic Data and Nuclear Data Tables **59**, 185 (1995)
[83] C. Y. Wong, Phys. Rev. Lett. **31**, 766 (1973)
[84] G. G. Adamian, N. V. Antonenko, and W. Scheid, Phys. Rev. C **68**, 034601 (2003)
[85] A. B.Migdal. Theory of finite fermi systems, and applications to atomic nuclei. Interscience Publishers, 1967.
[86] D. C. Hoffman, M. M. Fowler, W. R. Daniels, H. R. von Gunten, D. Lee, K. J. Moody, K. Gregorich, R. Welch, G. T. Seaborg, W. Brüchle, M. Brǧger, H. Gaggeler, M. Schadel, K. Sümmerer, G. Wirth, T. Blaich, G. Herrmann, N. Hildebrand, J. V. Kratz, M. Lerch, and N. Trautmann, Phys. Rev. C **31**, 1763 (1985).
[87] J. Li, X. Tang, and G. Wolschin, Physics Letters B **105**, 107 (1981)
[88] L. Zhu, J. Su, and P. W. Wen, Phys. Rev. C **95**, 044608 (2017)
[89] R. Bass, Phys. Rev. Lett. **39**, 265 (1977)